

# V723 Cas (Nova Cassiopeiae 1995): MERLIN observations from 1996 to 2001

I. Heywood<sup>1,2</sup>, T. J. O’Brien<sup>1</sup>, S. P. S. Eyres<sup>3</sup>, M. F. Bode<sup>4</sup>, R.J. Davis<sup>1</sup>

<sup>1</sup>University of Manchester, Jodrell Bank Observatory, Macclesfield, Cheshire SK11 9DL, UK

<sup>2</sup>University of Oxford Astrophysics, Keble Road, Oxford, OX1 3RH, UK

<sup>3</sup>Centre for Astrophysics, University of Central Lancashire, Preston, PR1 2HE, UK

<sup>4</sup>Astrophysics Research Institute, Liverpool John Moores University, Twelve Quays House, Egerton Wharf, Birkenhead, CH41 1LD, UK

Accepted 200x month xx. Received 200x month xx

## ABSTRACT

MERLIN observations of the unusually slow nova V723 Cas are presented. Nine epochs of 6 cm data between 1996 and 2001 are mapped showing the initial expansion and brightening of the radio remnant, the development of structure and the final decline. A radio light curve is presented and fitted by the standard Hubble flow model for radio emission from novae in order to determine the values of various physical parameters for the shell. The model is consistent with the overall development of the radio emission. Assuming a distance of  $2.39 (\pm 0.38)$  kpc and a shell temperature of 17000 K, the model yields values for expansion velocity of  $414 \pm 0.1$  kms<sup>-1</sup> and shell mass of  $1.13 \pm 0.04 \times 10^{-4} M_{\odot}$ . These values are consistent with those derived from other observations although the ejected masses are rather higher than theoretical predictions. The structure of the shell is resolved by MERLIN and shows that the assumption of spherical symmetry in the standard model is unlikely to be correct.

**Key words:** stars: individual: V723 Cas – novae, cataclysmic variables – stars: winds, outflows – radio continuum: stars

## 1 INTRODUCTION

Classical novae are interacting binary systems and the most energetic type of cataclysmic variable. The central system consists of a white dwarf primary and a main sequence secondary which fills its Roche lobe. Hydrogen-rich matter is accreted from the secondary onto the white dwarf via an accretion disc. Once the pressure at the base of the accreted envelope reaches a critical level, thermonuclear reactions begin under degenerate conditions leading to an explosion (Starfield 1989). As a direct result the bolometric luminosity of the system increases by at least three orders of magnitude over a timescale of a few days. Observational estimates of the mass of material ejected are typically  $10^{-5} - 10^{-4} M_{\odot}$  with velocities in the range a few hundred to several thousand kms<sup>-1</sup>. Correlations exist between the rate at which the visual light declines from maximum and the peak absolute magnitude and the ejection velocity. These are in the sense that the novae which fade most rapidly (“fast novae”) are intrinsically brightest and eject material at the highest speeds.

V723 Cas (Nova Cassiopeiae 1995) was discovered at  $V = 9.2$  mag on 1995 August 24 by M. Yamamoto (Hiro-sawa et al 1995) which for the purposes of this paper will be defined as day zero. The nova reached visual maximum of

$V = 7.1$  mag 115 days later on December 17. The light curve characteristics of V723 Cas display very slow evolution with a long pre-maximum halt (Hachisu & Kato 2004) and have led it to be classified as a very slow nova alongside HR Del and RR Pic (Chochol & Pribulla 1997). Oscillations in the light curve are evident post-maximum, a feature also seen in the evolution of HR Del. Optical spectroscopy (Iijima, Rosino & Della Valle 1998, Munari et al 1996) prior to maximum light revealed fairly narrow emission components (full width half maximum FWHM  $\sim 90$  kms<sup>-1</sup>) with P Cygni absorptions blueshifted  $\sim 100$  kms<sup>-1</sup> relative to the emission peak. Munari et al (1996) report that post-maximum the emission lines increase by a factor of several times in intensity and broaden to FWHM  $\sim 550$  km s<sup>-1</sup> whilst the absorption components remain at a similar width to pre-maximum. Ground and space-based infrared observations (Evans et al 2003) show line profiles with FWHM  $\sim 330$  km s<sup>-1</sup> and indicate an ejected mass of  $2.6 \times 10^{-5} M_{\odot}$  from the Br $\alpha$  line and  $4.3 \times 10^{-4} M_{\odot}$  from the free-free emission (assuming a distance of 4 kpc).

Radio emission in novae typically arises due to free-free emission from gas at temperatures of approximately  $10^4$  K (Seaquist 1989). Non-thermal components have been detected in a few novae, the most notable example being

**Table 1.** Summary of the MERLIN observations of V723 Cas.

Observation date	Wavelength (cm)	Days since discovery	Fitted Beam Size (mas×mas)	Fitted Beam PA (degrees)	Flux Density (mJy)
1996 Dec 13	6	477	55.3 × 44.5	−77.6	2.3 (± 0.5)
1997 Jan 25	6	520	51.3 × 44.1	54.8	2.4 (± 0.4)
1998 Mar 04	6	923	57.8 × 44.7	−29.2	7.0 (± 0.2)
1998 Apr 06	18	956	147 × 126.3	−29.3	4.3 (± 0.3)
1998 Dec 07	6	1201	162.5 × 54	1.7	8.2 (± 0.5)
2000 Feb 27	6	1648	124 × 52.9	28.9	7.9 (± 0.4)
2000 Apr 16	6	1697	54.8 × 35.7	−34.7	13.5 (± 0.9)
2001 Jan 29	6	1985	124.5 × 45.6	33	6.3 (± 1.1)
2001 Jun 03	6	2110	139.3 × 65.3	15.1	4.0 (± 0.7)
2001 Oct 26	6	2255	46.7 × 41.3	−89.8	5.4 (± 0.3)

GK Per which exhibits a non-thermal ridge coincident with the south-west portion of the optical shell (Bode, O’Brien & Simpson 2004). This is generally attributed to the collision between the nova ejecta and the previously shed common-envelope of a pre-nova phase, most likely following a ‘born-again’ AGB star phase (Dougherty et al 1996). Higher temperature emission detected in some nova outbursts (e.g. QU Vul, Taylor et al. 1987; V1974 Cyg, Pavelin et al 1993) suggests that, at least for some novae, there is shocked material within the ejected shell.

This paper presents results obtained from ten MERLIN observations of V723 Cas, nine at a wavelength of 6 cm and one at 18 cm. The 6 cm epochs produce maps and the shell structure is discussed. Radio flux measurements lead to a determination of the radio light curve to which standard models are fitted in order to determine values for the physical parameters of the nova outburst.

## 2 OBSERVATIONS

V723 Cas was observed using MERLIN between 1996 December 13 and 2001 October 26 resulting in ten epochs of data. A summary of the observations can be found in Table 1. The fitted beam is a 2D Gaussian fit to the point spread function for each observation.

The observing wavelength was 6 cm (4994 MHz) for all epochs except 6 April 1998 when it was 18 cm (1658 MHz). The nova was observed in phase-referencing mode, switching to phase-reference source 0102+511 (J2000) at regular intervals. The point source OQ208 was used as an amplitude calibrator and was flux calibrated against 3C286 using the Baars scale (Baars et al 1977). The data were edited and flagged using the MERLIN package DPLOT and the flux scale for each epoch was calibrated using DPROC. Further calibration, mapping and analysis was performed using AIPS. Each epoch was mapped to a  $512 \times 512$  pixel image. The phase-calibrator was also mapped using three passes of self-calibration. Due to the relatively weak emission from V723 Cas the phase-solutions from the phase calibrator were used to correct the data as self calibration was not possible. The data were also reweighted to allow for differences in the sensitivities of the telescopes in the MERLIN array.

## 3 RESULTS

### 3.1 The 6 cm radio maps

The nine radio maps at 6 cm are presented in Figure 1. Natural weighting of the data was used during mapping to maximise the signal to noise ratio and the CLEANING process was terminated when the total CLEANED flux reached a maximum value. A 50 mas circular restoring beam was used to create each map.

The December 1996 and January 1997 maps show that the source is unresolved by MERLIN at this early stage. As the shell expands over the next few epochs it appears to become extended along a north-south direction. Over a year later in February 2000 this north-south axis is still apparent although it now gives the appearance of being one side of a partial shell. The April 2000 data are rather noisy (see section 3.2) and only the two brightest peaks aligned with the north-south ridge are believed to be real emission from V723 Cas. The next image, taken 9 months later in January 2001, suggests that the north-south components have been replaced by ones aligned east-west. This structure then fades over the remaining two epochs.

### 3.2 Radio flux densities

Two methods were used for estimating the total flux density at each epoch. Firstly, the total flux density in the region of the source in the final CLEANED map was measured using IMSTAT and the uncertainty was determined from the rms variation in an off-source region of the map. Secondly, the area was re-imaged using UVTAPER to weight down the longer baselines. Tapering values of 500 k $\lambda$ , 1000 k $\lambda$  and 2000 k $\lambda$  were applied to the data and the data were also imaged with no tapering. This is particularly useful at epochs where the source is resolved since in these circumstances an interferometer cannot fully sample all the scale-sizes within the source. A Gaussian was then fitted to the source using IMFIT and the total flux density in this Gaussian and its uncertainty were recorded. The clean depths used for each of the methods were  $1\sigma$ ,  $2\sigma$  and  $3\sigma$  and the data were also imaged by cleaning down to the first negative clean component. The ten final flux measurements used from the set of 160 produced by these methods were chosen on the basis of the single imaging method which consistently gave the highest flux density. Using the two techniques allows an appreciation of the systematic uncertainties in the fluxes and

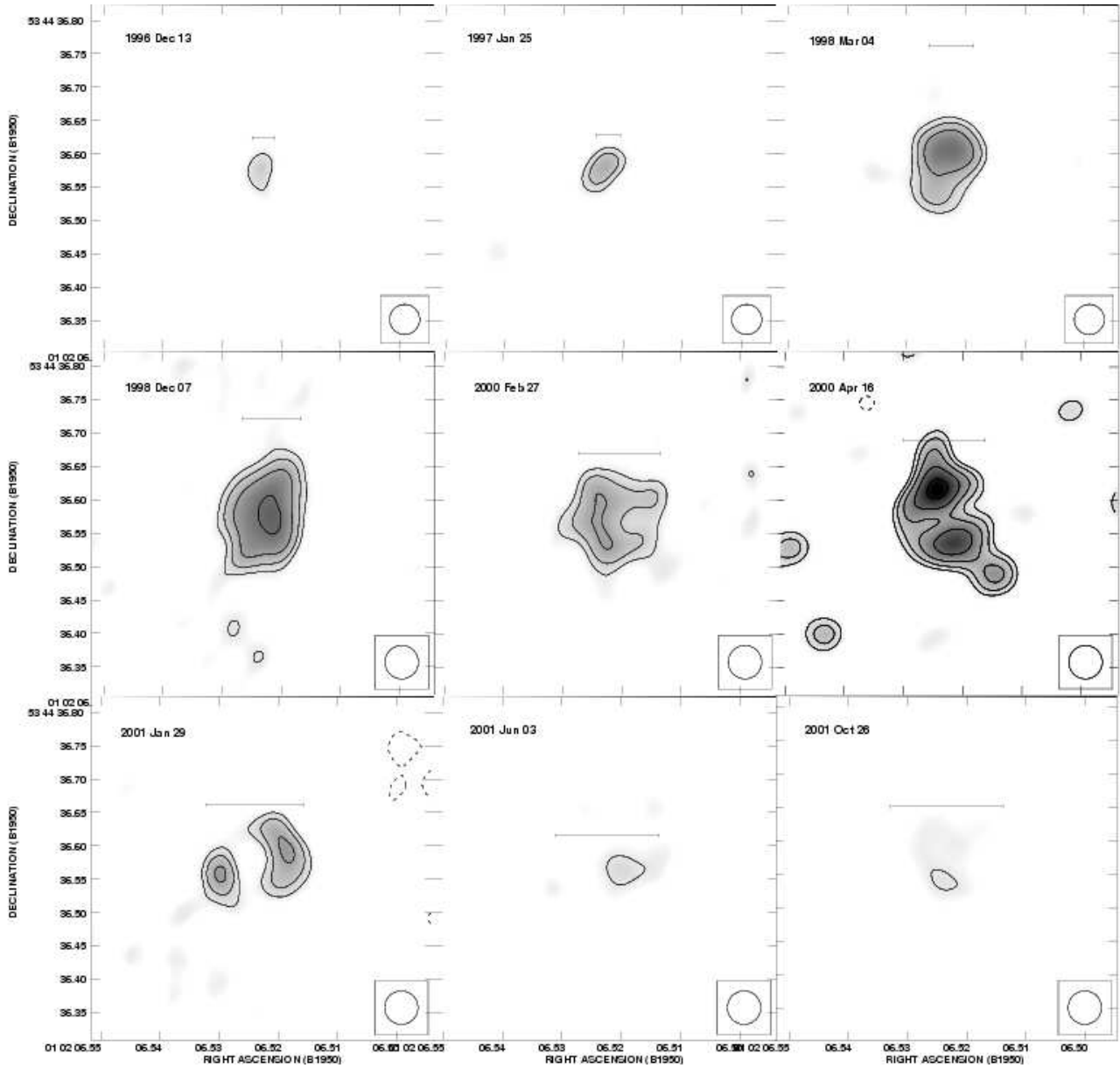


**Figure 1.** 6 cm MERLIN maps of V723 Cas. The contour levels are  $(-3, 3, 3\sqrt{2}, 6, 6\sqrt{2}, 12, 12\sqrt{2}\dots) \times 0.15$  mJy. The greyscale runs from 3 mJy to 20 mJy. The horizontal bars show the expected diameter of the shell assuming a particular distance and expansion velocity as discussed in the text.

leads to the estimates presented in Table 1. Figure 2 shows the resulting radio light curve for V723 Cas. The April 2000 observation appears to have unusually high flux density. Examination of the flux density of the phase calibrator reveals that it is also suspiciously high and that the data has poor phase calibration as a result. It is highly unlikely that the flux density value for this epoch is trustworthy.

## 4 INTERPRETATION

### 4.1 The radio light curve

The radio light curve is consistent with the classic 3-phase evolution for nova light curves (Hjellming 1990). The expanding shell is assumed to emit via thermal bremsstrahlung. In the earliest stages, Phase I, the shell is optically thick and the observed flux increases as the shell expands, the photosphere being coincident with the physical shell boundary. The flux is therefore expected to be proportional to  $\nu^2 t^2$ , where  $\nu$  is the frequency of the radio observation and  $t$  is the time since outburst. During Phase II the

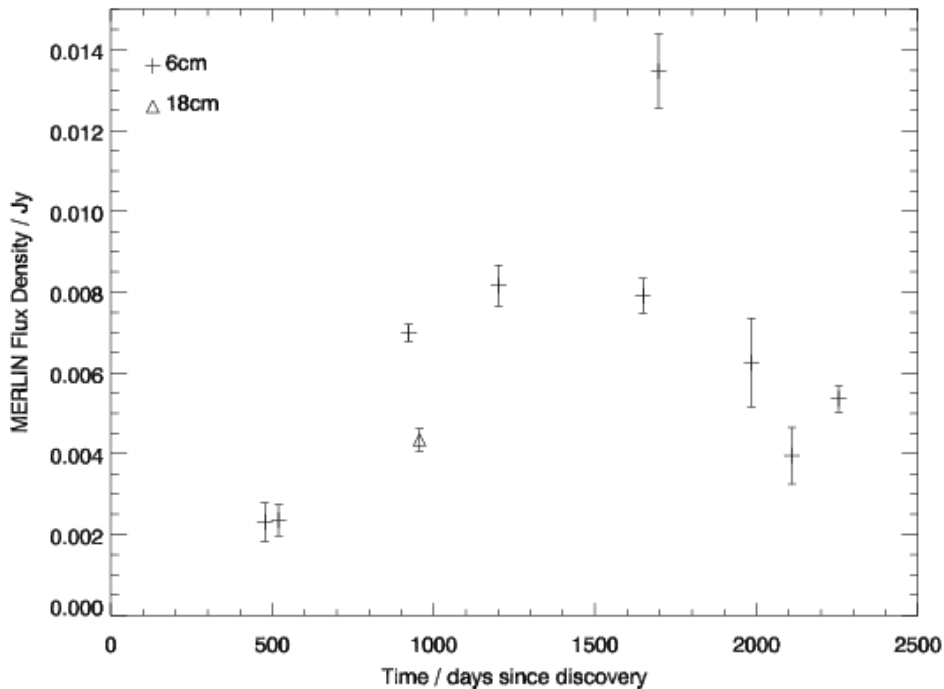


**Figure 2.** Radio light curve for V723 Cas. Nine 6 cm epochs and one 18 cm epoch are presented. Note the discussion in the text about the anomalously high flux density at day 1697.

effective photosphere lags behind the physical shell boundary as the shell becomes optically thin. Eventually the shell is entirely optically thin and, if it is isothermal, the flux declines as  $\nu^{-0.1}t^{-3}$ . Hjellming suggests that the flux in Phase II varies approximately as  $\nu^{0.6}t^{-4/3}$ .

It is possible to make a simple check on the spectral index of the emission using the flux densities from the contiguous observations on 1998 March 4 at 6 cm and on 1998 April 6 at 18 cm. This leads to a spectral index of 0.54 which implies that the turnover into optically thin emission has begun by this stage. However, by using the 6 cm flux density from March 4 rather than April 6 the spectral index is underestimated. This is consistent with the simple model proposed by Hjellming which predicts a spectral index between 0.6 and 2 for this phase of the evolution.

#### 4.2 Hubble flow model for radio emission from novae

By fitting a model for the emission to the light curve of Figure 2 it is possible to estimate the values of a number of physical parameters such as the mass of the shell and its ejection velocity. The standard model employed here is known as the Hubble flow model (Seaquist and Palimaka 1977; Hjellming et al. 1979). It assumes an isothermal spherically-symmetric shell resulting from an instantaneous mass ejection with a linear velocity gradient. Hence as the shell expands it grows thicker with internal and external boundaries determined by the assumed range of ejection velocities.

In each case the flux density expected at a given epoch and frequency is calculated by integrating the radiative

**Table 2.** Parameters for the Hubble flow model assuming a shell temperature of 17000 K and a distance of 2.39 kpc.

Model parameter	Best-fitting value
Ejected mass $M_e$	$1.13 \pm 0.04 \times 10^{-4} M_\odot$
Outer shell velocity $v_1$	$414.4 \pm 0.1 \text{ km s}^{-1}$
Inner shell velocity $v_2$	$102 \pm 4 \text{ km s}^{-1}$

transfer equation through the shell assuming a temperature and distance. The predicted values are then compared with the 6 cm observations (excluding the dubious 2000 April observation) and a chi-squared minimisation is used to estimate the best-fitting values of the parameters.

We estimate the temperature of the radio-emitting shell for use in the model-fitting by converting the peak flux density in the optically-thick 1996 December map to an equivalent brightness temperature of 17000 K. The distance is taken to be 2.39 ( $\pm 0.38$ ) kpc (Chochol & Pribulla 1997).

Best-fitting values of the model parameters are listed in Table 2. The reduced chi-squared value is 1.6 indicating a satisfactory fit to the data. We discounted the possibility that the fitting routine has become trapped in a local minimum of the  $\chi^2$  hyperspace by gridding the  $\chi^2$  values at high resolution. The uncertainties on the best-fit values for each parameter quoted in Table 2 are determined from marginalised likelihood distributions of  $\chi^2$  derived from a gridded region of parameter space around each best-fit position. For the Hubble flow model we can deduce from this method that the ejected mass, the shell velocity and the ra-

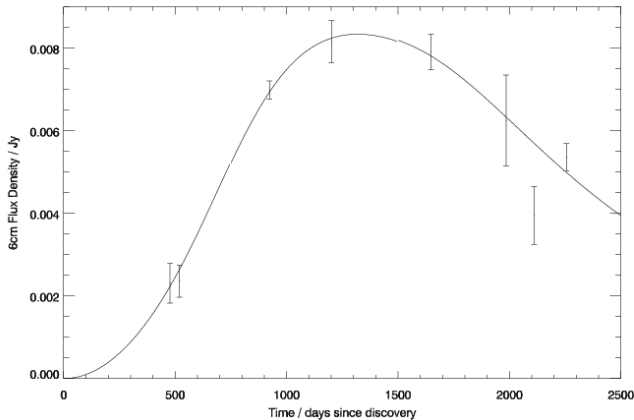


**Figure 3.** Best fitting model light curve for the Hubble flow model overlaid on the flux density measurements from the 6 cm MERLIN observations.

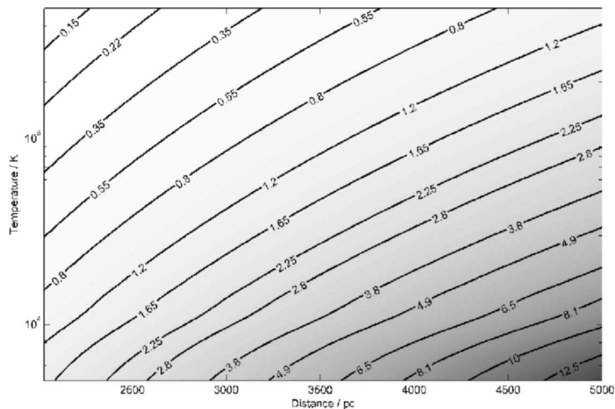


**Figure 4.** Best fitting mass contours for a range of temperatures and distances. The best fitting mass at any point in the plane is the contour value  $\times 10^{-4} M_{\odot}$ .

tio of inner to outer velocity are all well constrained and that the likelihood peaks at the best fit value.

Figure 3 shows the best fitting Hubble flow model light curve. The best fit for these models depends on both the distance to the nova and the temperature. Figures 4 and 5 show how the values of mass and velocity vary for different pairs of temperature and distance. The ratio of inner to outer velocity is fixed at 0.248 for all these model runs. These plots are the result of 10000 model runs resulting from 100 values each for temperature and distance.

The estimate of ejected mass derived from the radio lightcurve modelling of around  $1.1 \times 10^{-4} M_{\odot}$  is about 25% of that obtained from the free-free infrared continuum observations of Evans et al (2003). However they assume that the distance is 4 kpc. At the same temperature (17000 K), Figure 4 shows the ejected mass estimate from the radio emission rises to around  $4 \times 10^{-4} M_{\odot}$ . However, for this distance, assumption of a higher temperature (Evans et al use a value of  $3.2 \times 10^5$  K) would reduce the mass estimate again to around  $0.8 \times 10^{-4} M_{\odot}$ . As Evans et al (2003) point out, the estimates derived observationally are generally about an order of magnitude greater than those resulting from simulations of the thermonuclear runaway.

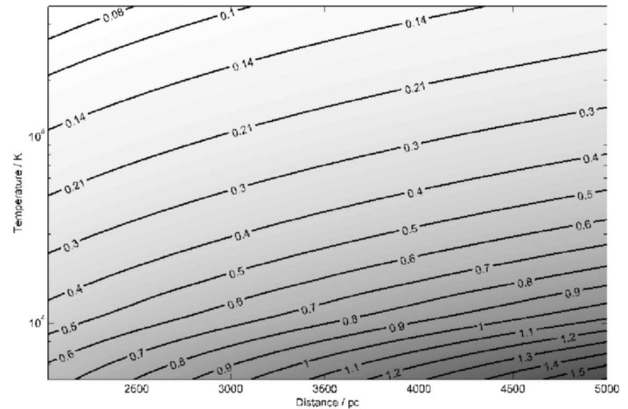


**Figure 5.** Best fitting velocity contours for a range of temperatures and distances. The best fitting velocity is the contour value  $\times 1000 \text{ km s}^{-1}$ .

The higher temperature cited above is thought to arise from ‘coronal’ gas around the nova. It is unlikely that this component of the ejecta makes anything other than a negligible contribution to the radio flux of the nova. This claim is based on the fact that RS CVn stars have radio fluxes comparable to that of a nova shell arising from coronal gas at temperatures in excess of  $10^8$  K (Hjellming & Gibson, 1980; Kuijpers & van der Hulst, 1985). It is therefore unlikely that coronal gas at  $3.2 \times 10^5$  K would significantly affect the results presented in this paper, although inclusion of this emission is an aspect which would improve the accuracy of future models.

Despite the reasonable fit to the radio light curve the Hubble Flow model cannot be an entirely accurate representation of the truth. The smooth mass distribution which the model is based on is misleading as images of nova shells, including the radio maps presented in this paper, show that the ejecta are far from uniform. In reality the material is highly clumped with polar and equatorial features of enhanced density (e.g. Harman & O’Brien 2003).

A simple statistical treatment for the clumping of the ejecta has been applied to investigate the effects that a non-uniform distribution of material may have on the best fitting parameters of the shell model. A similar method has been used to investigate mass-loss from OB stars (Abbott, Biegging & Churchwell 1981) and from Wolf-Rayet stars (Nugis, Crowther & Willis 1998). A correction factor is applied to the optical depth equations when solving the radiative transfer through the shell. The correction factor is governed by two parameters;  $x$  is the ratio of the lower density background to the high density clumps, and  $f$  is the filling factor, the fractional volume occupied by the high density clumps, or alternatively the fractional length along any line of sight which passes through the high density material. In this case, for  $x \geq 0.3$  the clumping changes the parameters by no more than a few percent, however for strong clumping ( $x \sim 0.01$ ,  $f \sim 0.01$ ) the best fitting mass can drop to approximately one third of the smooth shell case. The velocity of the outer shell boundary may increase by  $\sim 7\%$  for strongly clumped shells although generally the effect on this parameter is very small, probably due to it being well constrained during the optically thick stage. The inner shell velocity increases by up to a factor of 3 as  $f$  and  $x$  decrease, suggesting that increasing the density condensations in this model results in a

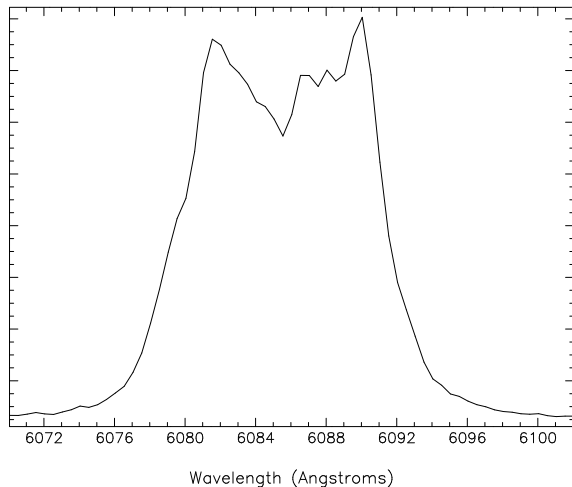


**Figure 6.** [FeVII] line for V723 Cas from O’Brien et al (in prep). The flux scale is relative and the data were taken on 1999 February 4 with the Intermediate Dispersion Spectrometer on the Isaac Newton Telescope.

thinner shell. A more thorough investigation into clumping in nova shells has been made by Heywood (2004).

### 4.3 Structure of the remnant

The apparent angular size of the expanding remnant can be estimated from the expansion velocity and distance. Expansion velocities are measured spectroscopically from the [FeVII] (6087 Å) line profile presented in Figure 6 (from O’Brien et al, in preparation). This forbidden line is chosen because it is optically thin and has a well-defined double-peaked structure. The expansion velocity can be measured from either peak to peak separation, full width at half maximum (FWHM) or the full width at zero intensity (FWZI). In this case these are  $210 \text{ km s}^{-1}$ ,  $290 \text{ km s}^{-1}$  and  $660 \text{ km s}^{-1}$  respectively. In the analysis below the peak to peak value is used as it probably represents the velocity of the majority of the ejected mass. Acceleration is assumed to be negligible for this calculation.

The radio lightcurve modelling resulted in velocities ranging from  $102$  to  $414 \text{ km s}^{-1}$  (inner and outer boundaries of the Hubble flow model) which is generally consistent with the velocities derived spectroscopically. For example, the early spectroscopy (Munari et al 1996, Iijima et al 1998) showed P Cygni absorptions at velocities about  $100 \text{ km s}^{-1}$  blueward of the emission peak, consistent with the lower velocities derived from the radio models. The expansion velocity derived from the average FWHM of the infrared emission lines (Evans et al 2003) of  $332 \pm 17 \text{ km s}^{-1}$  is slightly larger than the value derived above of  $290 \text{ km s}^{-1}$ .

The assumption that all material is ejected instantaneously with a linear velocity gradient is another feature of the Hubble-flow model which may be too simplistic. Spectroscopic analysis of nova shells indicates the presence of many velocity components. In some cases it appears that a relatively slow, high-mass component is embedded in a fast, tenuous wind. In this case, spectra of V723 Cas from 1996 August show a component at very high velocity of

$\sim 1500 \text{ km s}^{-1}$  in the P Cygni profiles of both infrared and optical lines (Evans et al 2003, O’Brien et al, in preparation). It should also be noted that the spherically symmetric wind-like Hubble-flow model cannot be entirely correct as it produces flat-topped line profiles in the optically-thin stage rather than the double-peaked profile seen in Figure 6. Future versions of these models will attempt to take these features into account.

Using a distance of  $2.39 (\pm 0.38) \text{ kpc}$  and an expansion time measured from the date of discovery (as the exact date of the outburst is unknown) the horizontal bars shown in Figure 1 represent the predicted angular size of the remnant at each epoch. Care must be taken when comparing the spectroscopically calculated angular sizes with the extent of the contours on the radio images. In later epochs the outer regions of the shell have faded below detectable levels so comparing the size of the outer contours with the bar is futile. This comparison is valid in the optically thick phase where the predicted angular sizes are generally in good agreement with the radio contours.

It would be interesting if the radio contours could be used to determine the distance to the nova from expansion parallax. This would be difficult since the radio contours do not accurately represent the size of the object beyond the optically thick regime. A detailed model to fit the radio contours would have to be implemented in order to estimate the distance. This will be addressed in a paper to follow.

An interesting effect is seen between the 2000 April and 2001 January observations. The north-south structure appears to be replaced by an east-west alignment of the brightest peaks. A possible explanation for the switching of the dominant emission axis involved optical depth effects caused by the ejecta being non-uniform. Initially the ejecta are optically thick so in the early radio observations only the photosphere is visible. The brightness of the source is dependent only upon its temperature and angular size. As the remnant expands the density decreases and the radio photosphere begins to lag behind the physical shell boundary. This is the point where structure in the shell may become evident in the radio observations. However, the higher density regions scattered throughout the shell would remain optically thick for longer than the low density regions and would appear as bright peaks in the radio maps. As the expansion continues it is possible that the bright peaks that appear in one observation may become optically thin and be replaced by high density regions at different positions in the shell giving the impression that the axis of the dominant emission regions has rotated. Nova shells are known to exhibit coherent regions of increased density such as polar caps and tropical rings (e.g. FH Ser – Gill & O’Brien, 2000) and these features would be ideally placed for the apparent north-south / east-west switching observed between epochs.

This apparent rotation is an effect that has been seen in other interferometric observations of classical novae e.g. V1974 Cyg (Eyres et al 1996) and V705 Cas (Eyres et al 2000). The 6 cm maps for V1974 Cyg show north-south structure developing for the first five epochs only to be replaced by east-west features in the final epoch. The corresponding 18 cm maps show the same effect but occurring at a later time. Since the emission at 18 cm will become optically thin at a later time than the 6 cm emission this may support the hypothesis that an optical depth effect is responsible.

However interpretation of radio interferometry maps is complicated since emission on certain scales can be ‘resolved out’ and the incomplete sampling of the  $uv$  plane means that the beam shape significantly influences the image. Structures on the scales seen in these maps are particularly prone to these sort of instrumental effects. Further progress in their interpretation will only be gained by simulated interferometric images of model shells which has been carried out and will be presented in a paper to follow.

## 5 CONCLUSION

Radio emission from V723 Cas has been detected at both 6 cm and 18 cm 477 days after discovery of the nova and has been monitored for a further 1778 days. The radio maps show non-uniform structure with a N-S ridge feature that develops over time and splits into two peaks which then switch to E-W alignment in the next map. The radio light curve is consistent with the evolution of other novae of faster speed classes.

A simple Hubble-flow model is applied to the radio flux measurements yielding values for expansion velocity ( $414.4 \pm 0.1$ )  $\text{kms}^{-1}$  and shell mass ( $1.13 \pm 0.04$ )  $\times 10^{-4} M_{\odot}$  for a distance of 2.39 ( $\pm 0.38$ ) kpc and temperature 17000 K. Although the value for ejected mass is consistent with previous estimates for classical novae there is still significant discrepancy between the mass predicted from the theory of the outburst (e.g. Starrfield, Truran & Sparks 2000) and the mass derived from modelling of observations such as those presented in this paper. Expansion velocities are similar to those derived from spectroscopic observations although the latter show that certain assumptions of the standard Hubble-flow model for radio emission are naive.

Asphericity of the shell and clumping of the ejected material are evident in many novae and future models should take these factors into account. The radio maps show how the morphology of the shell evolves and further understanding of this will only be gained when simulated model images are convolved with the  $uv$  distribution of the array and true synthetic images are produced. This will also provide insight into how nova shells will be seen by the next generation of interferometry networks such as *e*-MERLIN.

## ACKNOWLEDGEMENTS

MERLIN is operated as a UK National Facility by the University of Manchester, Jodrell Bank Observatory, on behalf of the Particle Physics and Astronomy Research Council (PPARC). IH and MFB are grateful to PPARC for provision of a postgraduate studentship and Senior Fellowship respectively. IH also wishes to thank Peter Blake of the Department of Computer Science at the University of Manchester for his data handling experience.

## REFERENCES

Abbott D.C., Biegging J.H., Churchwell E., 1981, ApJ, 250, 645  
 Baars J.W.M., Genzel R., Pauliny-Toth I.I.K., Witzel A., 1977, A&A, 61, 99

Bode M.F., O’Brien T.J., Simpson M., 2004, ApJ, 600, L63  
 Chochol D., Pribulla T., 1997, Contributions of the Astronomical Observatory Skalnaté Pleso, 27, 53  
 Dougherty S.M., Waters L.B.F.M., Bode M.F., Lloyd H.M., Kester D.J.M., Bontekoe T.R., 1996, A&A, 306, 547  
 Evans A., Gehrz R.D., Geballe T.R., Woodward C.E., Salama A., Sanchez R. Antolin, Starrfield S.G., Krautter J., Barlow M., Lyke J.E., Hayward T.L., Eyres S.P.S., Greenhouse M.A., Hjellming R.M., Wagner R.M., Pequignot D., 2003, AJ, 126, 1981  
 Eyres S.P.S., Davis R.J., Bode M.F., 1996, MNRAS, 279, 249  
 Eyres S.P.S., Bode M.F., O’Brien T.J., Watson S.K., Davis R.J., 2000, MNRAS, 318, 1086  
 Gill, C. D., & O’Brien, T. J. 2000, MNRAS, 314, 175  
 Hachisu I., Kato M., 2004, ApJ, 612, L57  
 Harman D.J., O’Brien T.J., 2003, MNRAS, 344, 1219  
 Heywood, I., ‘Radio Emission from Classical Novae’, PhD Thesis, The University of Manchester, 2004  
 Hirosawa K., Yamamoto M., Nakano S., Kojima T., Iida M., Sugie A., Takahashi S., Williams G.V. 1995, IAU Circ., 6213, 1  
 Hjellming R.M., 1990, in Cassatella A., Viotti R., eds, Physics of Classical Novae, Proc. IAU Coll. 122. Springer-Verlag, Berlin, p. 169  
 Hjellming, R. M., & Gibson, D. M. 1980, IAU Symp. 86: Radio Physics of the Sun, 86, 209  
 Hjellming R.M., Wade C.M., Vandenberg N.R., Newell R.T., 1979, AJ, 84, 1619  
 Iijima T., Rosino L., Della Valle M., 1998, A&A, 338, 1006  
 Kuijpers, J., & van der Hulst, J. M. 1985, Astronomy & Astrophysics, 149, 343  
 Munari, U., Goranskij, V.P., Popova, A.A., Shugarov, S.Yu., Tatarnikov, A.M., Yudin, B.F., Karitskaya, E.A., Kusakin, A.V., Zwitter, T., Lepardo, A., Passuello, R., Sostero, G., Metlova, N.V., Shenavrin, V.I., 1996, A&A, 315, 166  
 Nugis T., Crowther P.A., Willis A.J., 1998, A&A, 333, 956  
 Pavelin P.E., Davis R.J., Morrison L.V., Bode M.F., Ivison R.J., 1993, Natur, 363, 424  
 Seaquist E.R., Palimaka J., 1977, ApJ, 217, 781  
 Seaquist E.R., 1989, in Bode M.F., Evans A., eds, Classical Novae. Wiley, Chichester, p. 143  
 Starrfield S., 1989, in Bode M.F., Evans A., eds, Classical Novae. Wiley, Chichester, p. 39  
 Starrfield A., Truran J.W., Sparks W.M., 2000, NewA Rev., 44, 81  
 Taylor A.R., Pottasch S.R., Seaquist E.R., Hollis J.M., 1987, A&A, 183, 38

This paper has been typeset from a  $\text{\TeX}$ / $\text{\LaTeX}$  file prepared by the author.